ARTICLE

Check for updates

Early Cretaceous marine incursions into South Atlantic rift basins originated from the south

Xingqian Cui [1,2 ✉], Brent Wignall[3], Katherine H. Freeman [4] & Roger E. Summons [2,1 ✉]

The breakup of Gondwana resulted in sedimentary deposits recording lacustrine to marine environmental transitions in the South Atlantic rift basins during the Early Cretaceous. Currently, ambiguity pervades our understanding of the timing and orientation of the initial seawater incursion. Here we investigated hydrocarbon biomarkers in sediments from two drill cores off West Africa with stratigraphic coverage from the Berriasian-Barremian to Albian. Based on biomarkers that can distinguish non-marine from marine-influenced settings, initial seawater influx occurred through the southern entrance across the Rio Grande Rise-Walvis Ridge during the early Aptian stage. Transitional conditions prevailed during the Aptian stage as the seawater incursion induced microbial community and environmental reorganization until the Albian when fully marine conditions prevailed. Overall, results of this study are valuable in deciphering the final opening of the South Atlantic Ocean, fulfilling the global comparison of paleoenvironments, and facilitating future petroleum exploration along the South Atlantic conjugate margins.

[1] School of Oceanography, Shanghai Jiao Tong University, Shanghai, China. [2] Department of Earth, Atmospheric and Planetary Sciences, Massachusetts Institute of Technology, Cambridge, MA, USA. [3] Shell Exploration and Production Company, Houston, TX, USA. [4] Department of Geosciences, The Pennsylvania State University, University Park, PA, USA. ✉email: cuixingqian@sjtu.edu.cn; rsummons@mit.edu

The evolution of the South Atlantic Ocean, a consequence of the break-up of Gondwana supercontinent in the Early Cretaceous, has attracted substantial attention since Alfred Wegener proposed the hypothesis of continental drift[1]. Situated between Africa and South America, the South Atlantic Ocean is narrowly defined as the region between the northern Ascension Fracture Zone and the southern Agulhas-Falkland Fracture Zone. Recent studies on the South Atlantic Ocean emphasized its early tectonic evolution and distinctive depositional environments. The South Atlantic Ocean is further sub-divided into northern and southern sectors, separated by the structural high—Rio Grande Rise-Walvis Ridge (RGR-WR)[2,3], which developed along part of the Florianopolis Fracture Zone (Fig. 1). The northern sector consisted of a series of conjugate rift basins along the African and Brazilian margins in the initial stages and is, therefore, denoted as South Atlantic rift basins (SARBs). It was postulated that seafloor spreading in the southern sector initiated ~138 Ma ago with rapid deepening to water depths >3000 m within the first 20 Ma years, while the tectonic evolution of the northern sector is more complicated[4,5] (Supplementary Note 1; Supplementary Fig. 1). Nonetheless, it is generally agreed that the northern sector recorded the final separation of South America from Africa. Additionally, the Cretaceous strata of the SARBs now host Earth's largest existing evaporite mineral deposits, whereas the accompanying and widespread anoxia in SARBs promoted the formation of organic-rich sediment with generation and preservation of a vast amount of petroleum[6–11]. Overall, tectonic processes dictate the co-evolution of basin properties and their aqueous and biogeochemical environments. We thus used a comprehensive organic geochemical approach to test conflicting models for the emergence of ocean connectivity and basin conditions that led to the accumulation of important mineral and energy resources.

Over past decades, specific attention has been paid to the Berriasian-Albian stages when the rift basins witnessed lacustrine-to-marine environmental transitions and the emplacement of extensive evaporite mineral deposits[2,12]. The SARBs are regarded as typically lacustrine in nature during Berriasian-Barremian times, whereas restricted-to-full marine conditions were established from the Albian and onward[8]. Seawater incursion, as the primary cause of the initial lacustrine-marine transition, is defined as seawater inflow into a restricted lacustrine basin, either through meandering channels, overflow or seepage across the geographic barriers. However, the earliest plausible "marine" signal has been reported in the early Berriasian[13], the latest Barremian[10,14], and the Aptian times[15]. These dates all significantly predate the breaching of the RGR-WR and the opening of the equatorial Atlantic seaway in the Late Cretaceous[8,15–17], leaving the timing of the initial marine incursion unresolved. Furthermore, despite numerous reports of marine signals in the pre-opened SARBs, there is little agreement regarding the locality of initial seawater incursion, whether northward through the Walvis Ridge or southward through the equatorial Atlantic seaway[2,4]. Other than ambiguous propositions concerning the timing, orientation, and definitive drivers of the marine incursion, the consequences for environmental and microbial ecosystem transition are even less clear. These uncertainties preclude a definitive verification of the intrinsic linkage between the late Aptian evaporate deposits, the early marine incursion, and the Early Cretaceous climatic fluctuations[18,19]. Furthermore, a clear understanding of the seawater incursion into the SARBs provides valuable insights on reconstructing the history of seawater incursions of the Black Sea, the Mediterranean Sea, the Red Sea, and the Proto-ParaTethys Sea[20–22].

Biomarkers, the fossilized remains of organic molecules synthesized by specific groups of organisms, have been shown to have
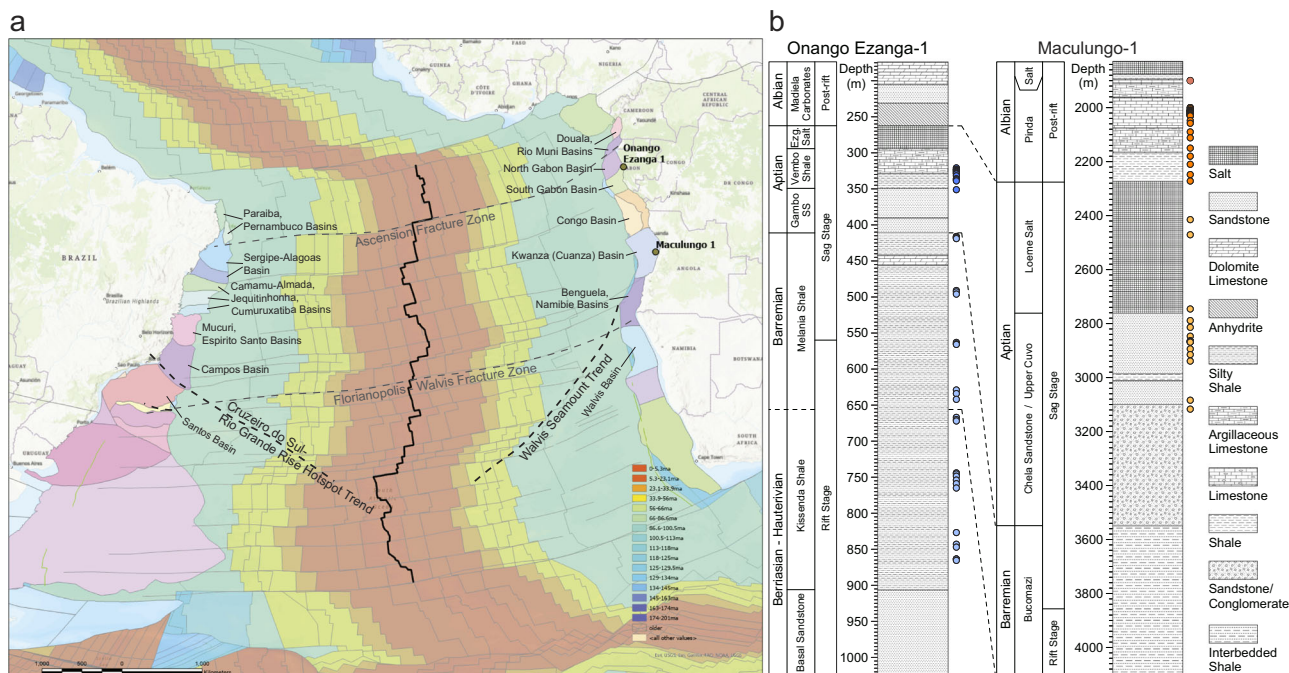
Fig. 1 Geographic locations and stratigraphy of two drill cores, Onango Ezanga-1 (ONEZ-1) and Maculungo-1 (MA-1). a Core locations where positional rift basins on both African and Brazilian margins are depicted in different colors. Major tectonic features (e.g., fracture zone) are annotated with gray and black dashed lines. The basemap was generated in ArcPro™ by adopting the plate reconstruction from the EarthByte 2019 plate model[73]. **b** Generalised stratigraphy with tectonic stages and drill core depths showing the placement of rock samples selected for this study. The stratigraphy and age models of both drill cores were revised from previous publications[52,53], by incorporating logging data with recent constructions of rift basin stratigraphy and age constraints[7,54,57,58]. Samples were selected randomly to avoid any lithologic bias. Drill core depths are presented in meters (m) below surface. Dark blue and light blue represent the Aptian and Berriasian-Barremian samples of the ONEZ-1 core, whereas dark orange and light orange indicate Albian and Aptian samples of the MA-1 core, respectively.

utility for reconstructing the nature and composition of ancient microbial communities which, in turn, are informative about depositional environments and water column chemistry[23–26]. In this study, we carried out biomarker analyses on two drill cores off West Africa to investigate the timing of the initial Early Cretaceous marine incursion, the associated environmental transitions, and the responses of microbial ecosystems. Our results reveal that the initial seawater incursion into SARBs commenced in the early Aptian time across the RGR-WR. Transitional conditions prevailed during the Aptian stage until fully marine conditions established in the Albian.

Biomarker proxies. Steroids and hopanoids are synthesized by a diverse range of eukaryotes and bacteria, respectively, and ratios of their degradation products, sterane/hopane, in sediments provide a semi-quantitative measure for the relative abundance of eukaryotes and bacteria[27,28] (Supplementary Table 1).

The highly informative but often not very abundant phytosterane, 24-*n*-propylcholestane (24-*n*pc; Supplementary Fig. 2), is the diagenetic product of 24-*n*-propylcholesterol and 24-propylidene-cholesterol, two major sterol constituents of pelagophyte algae[25]. Additionally, one foraminiferan has been shown to synthesize 24-propylidenecholesterol[29]. Given that all known pelagophytes and most foraminifera are marine organisms and that 24-*n*pc is ubiquitous in marine deposits, 24-*n*pc has been adopted as a diagnostic biomarker to indicate seawater influences. In practice, the detection and quantification of regular 24-*n*pc steranes may be confounded by signals from 4-methylstigmastane and dinosterane. Accordingly, the rearranged isomers of the 24-*n*pc (the 24-*n*pc diasteranes), unaffected by this interference, are adopted here for proxy calculation[21,30] (Supplementary Table 1).

In contrast to the wide occurrence of hopanoids in bacteria[31], the 2-methylhopanoids and their diagenetic products—2-methyl-hopanes—most likely record inputs from just two sources: cyanobacteria[32] and marine denitrifiers (i.e., *Methylobacterium salsuginis*)[33,34]. Similarly, the 3-methylhopanoids reflect two main sources[35]. Although minor groups of aerobic bacteria may synthesize trace amounts of 3-methylhopanoids under nutrient-limited conditions[36], 3-methylhopanes are most commonly applied as a biomarker for aerobic methanotrophy. They typically signify a strong methane cycle, especially in non-marine and other sulfate-deprived settings[6,37]. Gammacerane (Supplementary Fig. 2), derived from tetrahymanol synthesized by bacterivorous ciliates, has been widely adopted as an indicator for the intensity of water column stratification[38].

The sources of carotenoids, whether from phototrophic sulfur bacteria, cyanobacteria, or algae, are distinguishable based on the nature of the molecular assemblages[39]. Green sulfur bacteria (GSB) and purple sulfur bacteria (PSB) are the only known extant producers of chlorobactane and okenane precursors[40], respectively. Thus, the appearance of chlorobactane and okenane in ancient archives signifies highly stratified and euxinic water bodies[41–44]. When dominant, isorenieratane indicates low-light-adapted brown-colored strains of GSB occupying the deep euxinic photic zone[44]. When isorenieratane is accompanied by much higher amounts of renieratane and renierapurpurane, its source can be ascribed to cyanobacteria[39]. Additionally, a subset of cyanobacteria can synthesize synechoxanthin and its biosynthetic intermediates, which are preserved as diaromatic carotenoids with 38 and 39 carbon atoms[39,45,46], respectively.

While paleorenieratane lacks confirmation of its biological precursors, it can be attributed to GSB based on elevated carbon isotopic values similar to isorenieratane, which signal carbon assimilation via the reverse tricarboxylic acid cycle (rTCA)[47,48]. The β-series of aromatic carotenoids, including β-isorenieratene and β-renierapurpurin, precursors of β-isorenieratane and β-renierapurpurane, respectively, are synthesized by both photo-trophic sulfur bacteria and cyanobacteria[23,39,49,50]. β-carotane originates mostly from cyanobacteria, with lower amounts from algae. Because it is subject to similar taphonomic controls as the other carotenoids, it is a useful reference point and can be applied as the denominator when parameterizing carotenoid proxies[40,51].

Results

Study area and sampling. The 90 samples investigated in this study originated from two cores, being Onango Ezanga-1 (ONEZ-1) drilled in the Gabon Basin and Maculungo-1 (MA-1) from the Kwanza Basin (Fig. 1). The stratigraphy of each drill core was constructed from sedimentology logging (Supplementary Note 2). Whereas the constructed stratigraphy is consistent with recent proposals, it represents a modification from previous publications[7,52,53]. The age models for both drill cores were determined based on several stratigraphic markers, particularly the base of the Aptian stage (~121.4 Ma), and the lower (~114 Ma) and the upper (~113 Ma) boundaries of the Aptian evaporite deposits[2,54] (Supplementary Note 3). Explicitly, the "late Aptian" age model has been adopted in this study to reconcile the recent controversies[55–58] (Supplementary Note 3). Nonetheless, it is noteworthy that the choice of absolute ages does not change the conclusions of this study, particularly the relative timing of the seawater incursion in relation to the geological stages and to the Aptian evaporite deposits.

Samples from ONEZ-1 cover the Berriasian-Barremian (Berr/Bar) to Aptian stages, whereas MA-1 samples cover the Aptian to Albian stages (Fig. 1). Based on core descriptions and depositional stages, samples are separated into four groups: ONEZ-1 Berr/Bar, ONEZ-1 Aptian, MA-1 Aptian, and MA-1 Albian. A detailed thermal history assessment based on biomarker maturity proxies suggests that these sediment samples are either pre-mature (i.e., before oil generation) or in the early oil generation window (Supplementary Note 4; Supplementary Figs. 3, 4), at which maturity level biomarker indices remain robust for the interpretation of paleoecology and paleoenvironments.

Triterpenoid proxies. Sterane/hopane ratios are 0.12 ± 0.06 and 1.91 ± 1.61 in ONEZ-1 Berr/Bar and ONEZ-1 Aptian, and 1.53 ± 0.96 and 1.47 ± 0.90 in MA-1 Aptian and MA-1 Albian, respectively (Fig. 2). ONEZ-1 Aptian exhibits the highest fluctuation, and significant differences are observed between ONEZ-1 Berr/Bar and other groups of samples ($p < 0.001$). 24-*n*-Pro-pylcholestane is undetectable in ONEZ-1 Berr/Bar (Supplementary Fig. 5), suggestive of purely non-marine deposition. The proportions of 24-*n*pc (24-*n*pc/C_{27-30}; Supplementary Table 2) diasteranes in MA-1 Aptian ($2.07 \pm 0.85\%$) are notably higher than in ONEZ-1 Aptian ($1.03 \pm 1.08\%$; $p < 0.005$) and MA-1 Albian ($1.53 \pm 0.56\%$; $p < 0.05$) (Fig. 2).

As a semi-quantitative proxy, 2-methylhopane index (2-MHI; Supplementary Table 3) shows the lowest and highest values in ONEZ-1 Berr/Bar ($0.93 \pm 0.65\%$) and ONEZ-1 Aptian ($9.13 \pm 4.18\%$), respectively (Fig. 3). Albeit considerably lower 2-MHI values in ONEZ-1 Berr/Bar ($p < 0.001$), the other three groups are indistinguishable apart from the MA-1 Albian being lower than ONEZ-1 Aptian ($p < 0.01$). Values of 3-methylhopane index (3-MHI; Supplementary Table 3) are remarkably higher in ONEZ-1 Berr/Bar (8.30 ± 4.08) compared to the other three groups ($p < 0.001$) (Fig. 3). Gammacerane index shows the most pronounced values in ONEZ-1 Aptian (0.26 ± 0.26) and lowest values in MA-1 Albian (0.10 ± 0.06) (Fig. 2).

Carotenoid proxies. The sum of chlorobactane, okenane, paleor-enieratane and isorenieratane over β-carotane [(chl+oke+paleo+iso)/β-carotane], which represents the overall intensity of photic
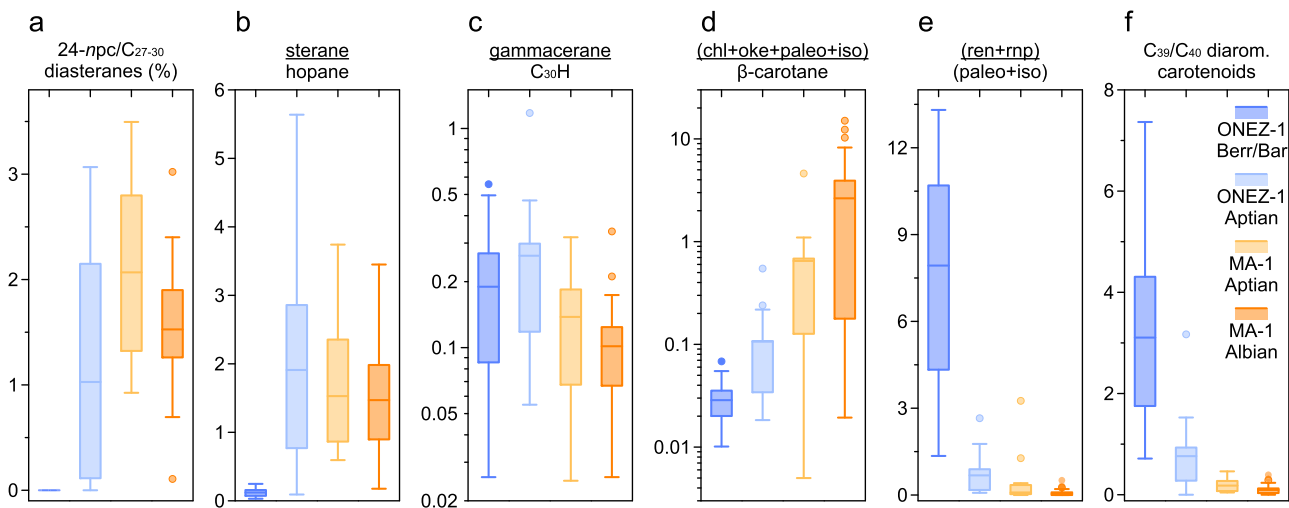
Fig. 2 Box-whisker plots for six biomarker proxies. a The percentage of 24-n-propylcholestane (24-npc) over C_{27} to C_{30} diasteranes, as defined in the Supplementary Table 1. **b** The relative abundance of sterane and hopane compounds. **c** Gammacerane over C_{30} $\alpha\beta$ hopane ($C_{30}H$). **d** The sum of chlorobactane (chl), okenane (oke), paleorenieratane (paleo), and isorenieratane (iso) relative to β-carotane. **e** The ratio of renieratane (ren) and renierapurpurane (rnp) relative to paleorenieratane and isorenieratane. **f** The relative abundance of C_{39} and C_{40} diaromatic carotenoids. Samples were separated into four groups based on wells and formations. Samples from Maculungo-1 (MA-1) were divided into Albian (MA-1 Albian) and Aptian (MA-1 Aptian), while samples from ONEZ-1 were divided into Aptian (ONEZ-1 Aptian) and Berriasian/Barremian (ONEZ-1 Berr/Bar). The lower and upper box boundaries for each group of data points represent first and third quartiles of the dataset, while the line within each box represents the mean value. The whiskers ("error-bars") are defined by 1.5 times of interquartile range (IQR), while colored dots are "outliers". The interpretation of each proxy is discussed in the main text and supplementary file.

zone euxinia (PZE), ascends sequentially in ONEZ-1 Berr/Bar (0.029 ± 0.014), ONEZ-1 Aptian (0.11 ± 0.13), MA-1 Aptian (0.65 ± 1.08) and MA-1 Albian (2.64 ± 3.82), with remarkable differences between every two groups ($p < 0.01$) (Fig. 2; Supplementary Table 4). C_{40} diaromatic carotenoid ratios of (renieratane + renierapurpurane)/(paleorenieratane + isorenieratane) [abbreviated here as (ren+rnp)/(paleo+iso)], as a proxy indicating the relative abundances of cyanobacteria and GSB, descend in order in ONEZ-1 Berr/Bar (7.93 ± 3.85), ONEZ-1 Aptian (0.68 ± 0.70), MA-1 Aptian (0.38 ± 0.80) and MA-1 Albian (0.08 ± 0.12) (Fig. 2). Ratios of C_{39} over C_{40} diaromatic carotenoids covary with (ren+rnp)/(paleo+iso), and display considerable differences between every two groups of samples (Fig. 2).

Discussion

Aromatic carotenoids as candidate proxies for paleoenvironmental discrimination

Our results reveal that lacustrine and marine settings exhibit distinct patterns of carotenoids (Fig. 4). While high abundances of aromatic carotenoids (e.g., isorenieratane, paleorenieratane, chlorobactane, okenane) have been reported for sediments deposited through geologic time, recent advances in analytical techniques permit carotenoid detection in trace levels[37,42]. ONEZ-1 Berr/Bar lacustrine shale sediments are characterized by low levels of aromatic carotenoids relative to β-carotane, of which the former is dominated by renierapurpurane, renieratane, and a group of C_{39} diaromatic compounds (Fig. 4). This is similar to patterns reported from representative cyanobacterial cultures, typical lacustrine sediments (e.g., Green River Shale) and most of the Proterozoic sediments deposited under low sulfate conditions[37,39,42]. Nevertheless, sulfate-rich lacustrine settings are an exception to the general non-marine pattern in situations where salinity, basin shape or other factors serve to inhibit the water overturn and where carotenoids may be dominated by GSB and PSB markers such as isorenierieatene, chlorobactene or okenone and their diagenetic products[21,37,43,59].

Under fully marine conditions, Albian sediments of the SARBs, despite containing cyanobacterial aromatic carotenoids at low levels, feature prominent isorenieratane, chlorobactane and a lower content of paleorenieratane, signifying predominant inputs from GSB. Patterns of carotenoids in Albian sediments are similar to many Phanerozoic marine PZE records, where aromatic carotenoids, when present, are dominated by chlorobactane or isorenieratane, or occasionally paleorenieratane, as in the Paleozoic.

When parameterizing aromatic carotenoids based on their origins from specific organisms, ratios of (ren+rnp)/(paleo+iso) and C_{39}/C_{40} diaromatic carotenoids show vastly different values in Berr/Bar (7.93 ± 3.85; 3.11 ± 1.86) and Albian (0.38 ± 0.80; 0.18 ± 0.14) sediments, respectively. In fact, ratios of (ren+rnp)/(paleo+iso) (7.93 ± 3.85) in Berr/Bar stage are comparable to values of 19.55 ± 14.00 in the lacustrine Green River Shale and the terminal Triassic lacustrine Bristol Channel Basin[24,37]. Furthermore, a shift toward lower (ren+rnp)/(paleo+iso) values was observed when the Bristol Channel Basin transitioned from a restricted lake to a marine-influenced basin[24]. Above distinction suggests that aromatic carotenoid-based proxies are valuable for distinguishing lacustrine versus marine settings.

Given their origins from cyanobacteria, renieratane, renierapurpurane and C_{39} diaromatics formed during diagenetic decarboxylation are putative "markers" of cyanobacteria under non-marine environments. Many cyanobacteria, predominantly non-marine taxa, synthesize the dicarboxylic acid synechoxanthin and some monocarboxylic acid biosynthetic precursors, as well as much higher levels of renierapurpurin and renieratene compared to isorenieratene, making their carotenoid inventories quite distinct from those of the phototrophic sulfur bacteria[39]. These patterns are consistent with phylogenetic profiling shows that *cruE* and *crtU* genes encoding enzymes essential for the biosynthesis of aromatic carotenoids are distributed across diverse taxa, whereas the *cruH* gene necessary for aromatic methyl groups to be oxidised to carboxyl is only present in cyanobacteria[23,45,46].

The reason why aromatic carotenoids are useful for discriminating between depositional environments can be rationalised by
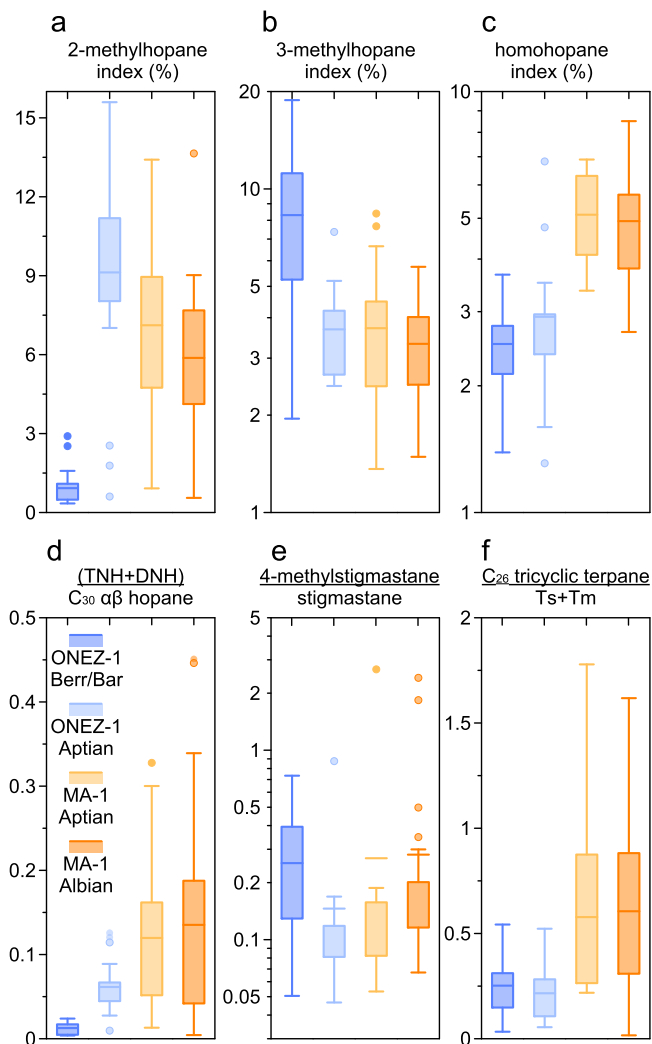
Fig. 3 Box-whisker plots for six sterane, hopane and tricyclic terpane biomarker proxies. a–c are 2-methylhopane index, 3-methylhopane index and homohopane index in percentage (%), respectively, as defined in the Supplementary Table 1. **d** The sum of trinorhopane (TNH) and 28,30-dinorhopane (DNH) over C_{30} αβ hopane. **e** The relative abundance of 4-methylstigmastane and stigmastane. **f** The ratio of C_{26} tricyclic terpane over 18α(H)-22,29,30-trinorneohopane (Ts) and 17β(H)-22,29,30-trinorhopane (Tm). Sample groups and plots were defined the same as in (Fig. 2). The interpretation of each proxy is discussed in the main text and the supplementary file.

the sulfate level and redox conditions of the waterbody. Oxygenic phototrophs, such as cyanobacteria, will predominate in a sulfate-lean waterbody (e.g., freshwater lacustrine) and this is recorded by high values of (ren+rnp)/(paleo+iso) and C_{39}/C_{40} diaromatic carotenoids, and low ratios of (chl+oke+paleo+iso)/β-carotane, the proxy reflecting the intensity of PZE. The reverse pattern is observed under sulfate-rich marine conditions, where synechoxanthin-producing cyanobacteria are sparse and PZE can develop to support GSB and PSB. The effectiveness of aromatic carotenoids in distinguishing lacustrine versus marine settings is further corroborated by its strong correlations with other paleoenvironmental proxies, such as sterane/hopane ratios, homohopane index (HHI; C_{35}/C_{31-35} homohopane), and 2-MHI (Figs. 3, 5; Supplementary Fig. 4), which all have been applied as empirical signals for separating lacustrine versus marine environments.

Early Aptian Initial marine incursion into SARBs. Debate surrounds the timing of initial marine incursions into the SARBs with current proposals that range from the early Berriasian to the late Aptian. The earliest marine signal in rift basins dates back to ~140 Ma based on the observation of "pelagic" limestones near the equatorial Atlantic Ocean[13]. However, such lithological features are more likely controlled by local topography, bathymetry, and particle provenance[60].

Micro- and macro-fossils provide another means of interpreting marine conditions. Late Barremian seawater incursion was reported in the Sergipe-Alagoas Basin, based on bivalves and fishes attributed to marine conditions[10,61]. Nonetheless, given the synchronous evolution of the conjugate margins[5], it contrasts with the observed non-marine ostracod assemblages in the conjugate Gabon Basin and the SARBs to the south in the Barremian-Mid Aptian[16], and the first occurrence of marine faunas in SARBs in the late Aptian[8]. However, the inflowing seawater that carried marine faunas by the late Aptian may largely postdate the initial seawater influx, relegating microfossils as less robust indicators for tracing the earliest marine incursion[16,62,63].

Seawater is essential to the growth of marine pelagophytes, which are geochemically recorded by the presence of the C_{30} sterane (24-npc) biomarker[25]. One of the earliest investigations in the Congo Basin reported 24-npc in all samples from the early Barremian to the Aptian[9,14], but as mentioned by these authors, these findings warrant careful re-evaluation of the 24-npc identification due to the likely interference from signals of the C_{30}-methylsteranes[21,64]. Similarly, 24-npc has been falsely identified in the northern interior seaway in the Aptian[65], given the criteria of 24-npc identification[21], which also questions the recognition of marine fossils in the Sergipe-Alagoas Basin migrated from the equatorial Atlantic seaway in the late Barremian[10,61]. Further, definitive reports of 24-npc at the Albian stage likely do not represent the earliest signals of marine incursion[66,67].

In the present study, the absence of 24-npc in Berr/Bar stages and its detection in the subsequent Aptian and Albian times demonstrate marine conditions prevailed in the SARBs as far back as the early Aptian (Supplementary Fig. 5). It confirms previous findings of 24-npc in early Aptian sediments in the Kwanza Basin[6]. The Aptian seawater incursion is additionally supported by declining ratios of (ren+rnp)/(paleo+iso) and C_{39}/C_{40} diaromatic carotenoids, pointing toward relatively higher sulfate levels and hence more "marineness" than Berr/Bar stages. Such postulation is further corroborated by diminishing 3-MHI in the Aptian (Fig. 3), which is suggestive of suppressed methanotrophic activity, most likely due to the competitive activity of sulfate-reducing microbiota[68] or progressively longer distance between study sites and the sites of methane seepage. Empirically, a low level of sulfate from seawater ingression is sufficient to oxidize methane generated below the chemocline. Based on the age range (~114–113 Ma; Supplementary Note 3) of evaporite deposition in the SARBs[2,11,18,56,69], and the ubiquitous detection of 24-npc in Gamba and Upper Cuvo formations underlying the Aptian evaporites, we therefore suggest that seawater incursions commenced before 114 Ma, but not earlier than the terminal Barremian (~121.4 Ma). Overall, the proposed timing of initial seawater incursion corroborates the continuous subsidence of the sag basins and the prevailing evidence on the evolution of the geographic barriers in the Aptian (Supplementary Note 1).

Northward seawater incursion across the RGR-WR. Southward seawater influx through the equatorial Atlantic Ocean gateway was initially proposed based on lithological evidence[13], and is further supported by evidence of macrofossils in the northern
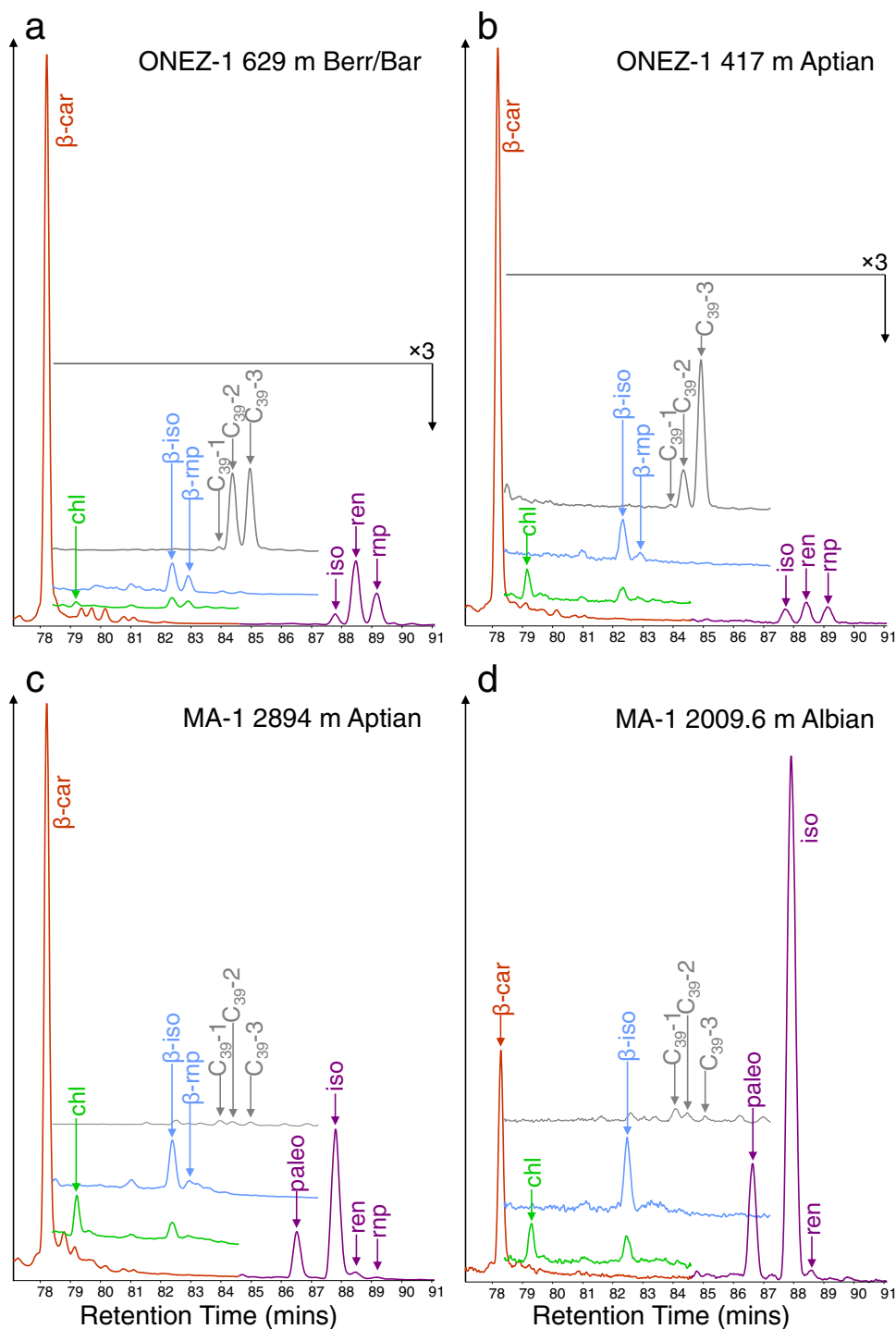
Fig. 4 Four representative chromatograms of carotenoid hydrocarbons. a, **b** are from samples of Aptian and Berriasian/Barremian (Berr/Bar) ages, respectively, from ONEZ-1 well, while (**c**) and (**d**) are samples of Albian and Aptian ages, respectively, from Maculungo-1 (MA-1) well. The lacustrine deposition, as of (**a**), is typified by high β-carotane (β-car) relative to aromatic carotenoids, while the marine deposition, as of (**d**) is characterized by high C_{40} aromatic carotenoids (e.g., isorenieratane—iso and paleorenieratane—paleo). β-iso: β-isorenieratane; β-rnp: β-renierapurpurane; C_{39}-1 to C_{39}-3: three diaromatic carotenoid isomers with 39 carbon atoms without definitive structures. See Fig. 2 for additional abbreviations.

basins[10,61]. Later investigations reported a rich array of evidence favoring either orientation, making the initial speculation ambiguous[8,11,16,65], primarily due to a lack of SARBs-wide comparison, as well as the robustness of proxies.

Biomarker observations may reveal the locality and orientation of the initial seawater incursion by assuming that seawater influx across barriers (e.g., RGR-WR) exerts a stronger influence on

water chemistry in proximal basins relative to those more distal, once SARBs were inter-connected as one giant waterbody in the early Aptian[5,15]. Despite the detection of 24-$n$pc in both basins in the Aptian stage, much higher proportions of 24-$n$pc, on average, are observed in the Kwanza Basin compared to the Gabon Basin ($p < 0.005$; Fig. 2), making these two basins simultaneously "marine" and "lacustrine", respectively. Although the discrepancy
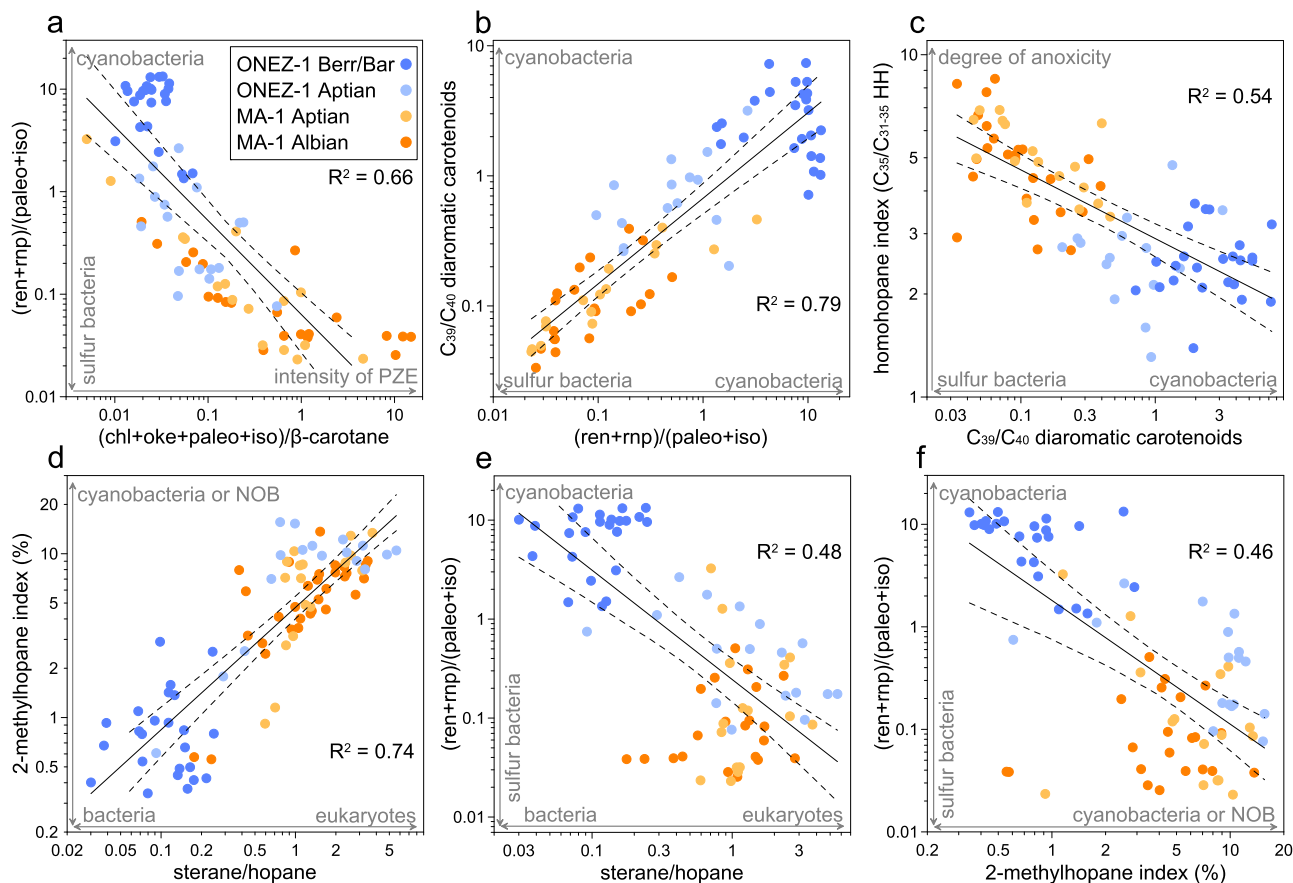
Fig. 5 Cross-plots of selected depositional environment and microbe-related biomarker proxies. a, b are correlations of carotenoid-derived proxies. **c** Homohopane index versus the ratio of C_{39}/C_{40} diaromatic carotenoids. **d** 2-Methylhopane index plotted against the ratio of sterane/hopane. The ratio of (ren+rnp)/(paleo+iso) versus (**e**) the ratio of sterane/hopane and (**f**) 2-methylhopane index. Samples are separated into the four groups described in the text. The inferred meaning of each ratio, explicitly (ren+rnp)/(paleo_iso)[24,39], (chl+oke+paleo+iso)/β-carotane[26], C_{39}/C_{40} diaromatic carotenoids[21,39], homohopane index[30], 2-methylhopane index[33], and sterane/hopane[27], is annotated with gray arrows and labels. The solid line and dashed lines represent best fitting curves and 95% confidence levels.

of 24-$n$pc abundance between these two basins is partially ascribed to drill core depth coverage of samples, regional topographic, and taxonomic biases, the occurrence of higher proportions of 24-$n$pc (2-3%) in sporadic stratigraphic intervals in the Gabon Basin suggests that marine pelagophyte growth, and thus the intensity of seawater influence, is unlikely biased by these factors. Accordingly, a higher abundance of 24-$n$pc, on average, likely reflects higher pelagophyte density, which is reasonably attributed to a more prominent seawater influence in the Kwanza Basin.

Patterns of carotenoids additionally corroborate the northward seawater incursion. Ratios of (chl+oke+paleo+iso)/β-carotane display higher values in the Kwanza Basin compared to the Gabon Basin in the Aptian (Figs. 2, 5), suggestive of stronger PZE in the southern basin. Under reducing conditions, the intensity of PZE may not be related to the efficiency of anaerobic sulfate reduction but likely driven by the sulfate inventory of an initially brackish waterbody. Therefore, the more intense PZE implies a larger sulfate pool and more saline conditions in the Kwanza than Gabon Basins in the Aptian stage. Less marine influence and lower sulfate levels in the northern basins are additionally in consensus with higher ratios of (ren+rnp)/(paleo+iso) and C_{39}/C_{40} diaromatic carotenoids in the Gabon than Kwanza Basins.

Values of HHI and their strong correlation with carotenoid proxies (Fig. 5 and Supplementary Fig. 3), together with (trinorhopane+dinorhopane)/C_{30} αβ hopane [(TNH + DNH)/C_{30}

αβ Hopane] ratios in representative of chemoautotrophic bacteria consuming sulfide[70] (Fig. 3), further support the postulation of a larger sulfate pool in the Kwanza Basin compared to the Gabon Basin. Despite moderate sulfate discharge from the surrounding catchment[63], the larger sulfate pool in rift basins, when corroborated by the detection of 24-$n$pc, is ascribed to seawater supply. Hence, the stronger marine influence, higher sulfate level, as well as the relatively weakened water column stratification based on gamma-cerane index (Fig. 2), in the southern Kwanza Basin than the northern Gabon Basin in the Aptian is attributed to the northward seawater influx through the southern barrier—RGR-WR in the early Aptian[18,62].

We additionally considered and negated the possibility of southward seawater incursion from the equatorial Atlantic seaway. Despite marine fossils being reported in the northern Sergipe-Alagoas Basin in the late Barremian[10,61], this is contradicted by the non-marine biomarker patterns in sediments of the northern interior seaway in the Aptian[65]. If northern SARBs witnessed the initial seawater incursion through the northern entrance in the Aptian, seawater signals should have been similarly recorded in the interior seaway. Furthermore, the signal of "less" marine influence was unlikely caused by riverine freshwater dilution in the tropical Gabon Basin under a humid climate[9,12]. First, the waterbody in Sergipe-Alagoas, Gabon, Kwanza, and Congo basins was hypersaline through the Aptian[11,14], as revealed by high gammacerane index values (>0.1; Fig. 2), suggestive of insignificant disproportional

bias by freshwater discharge. Second, salt deposition was observed in Gabon and the conjugate Sergipe-Alagoas basins in the Aptian[2,11,18,19], indicating higher evaporative water loss compared to freshwater supply. Third, the southward migration of a partially brackish water from the Gabon to Kwanza basins theoretically, when being diluted by drainage basin-supplied freshwater, weakens seawater signals in the Kwanza Basin, which contradicts our observation. Additionally, the breaching of the northern boundary, Ascension Fracture Zone, is later than that of the southern Walvis Ridge[4,71,72].

Overall, the interpretation of southern origin and northward progression of seawater incursion is consistent with published evidence of basin water chemistry, faunal migration and tectonic evolution. For example, earlier studies discovered more saline/brackish water conditions and thicker evaporite deposits in the southern rift basins[7,12]. Furthermore, the earliest marine microfossils were strongly affiliated with southern South Atlantic species in the latest Aptian stage followed by northward faunal migration, whereas the Northern Hemispheric taxa appeared later in the early Albian stage[8]. Despite disagreement with the modeled earlier rifting of the equatorial Atlantic Ocean[11,58], or the southward migrated rift extension[2], a southern origin and northward influence of seawater incursion is supported by the northerly propagated seafloor spreading reconstructed with plate tectonic models[73], the latest incipient opening of the equatorial Atlantic gateway in the Albian stage[3,4,19], and the bathymetric evolution of the geographic barriers (Supplementary Note 1; Supplementary Fig. 1). Additional evidence from the northern rift basins (e.g., Sergipe-Alagoas Basin) is needed to confirm this and to completely rule out the possibility of seawater incursion from the equatorial Atlantic in the Barremian and early Aptian.

Transitional seawater influence in the Aptian. Our results further reveal that the Aptian, with evidence of seawater incursion, represents a transitional stage during the early evolution of the SARBs (Figs. 2, 3). A previous study observed in the Aptian Kwanza Basin the precedence of 4-methylstigmastane over dinosterane, a pattern typical of freshwater conditions[6]. However, this contradicts our observation of elevated dinosterane/4-methylstigmastane ratios and declines in 4-methylstigmastane/stigmastane ratios from the Berr/Bar to the Aptian (Fig. 3; Supplementary Fig. 6). Additionally, the Congo Basin was proposed as a restricted marine basin in the late Aptian based on methyl-steranes and 28,30-dinorhopanane[14]. Without an examination of patterns in light of Berr/Bar and Albian stages, none of the above observations provided robust evidence in support of a transitional Aptian stage.

The Aptian stage is characterized by transitional features in between Berr/Bar and Albian stages in carotenoid biomarkers, nevertheless, differs significantly from bracketing stages in carotenoid-based proxies (Fig. 2). Ratios of (ren+rnp)/(paleo +iso) and C_{39}/C_{40} diaromatic carotenoids, as putative proxies for distinguishing lacustrine vs. marine conditions, closely mirror each other and decline exponentially from the Berr/Bar to Aptian and then Albian stages (Figs. 2, 4, 5). Consistent with patterns above, ratios of (chl+oke+paleo+iso)/β-carotene, indicative of PZE intensity, show similar intermediate values in the Aptian stage. Given that our Berr-Bar-Albian sediments were deposited under stratified and reducing conditions, as suggested by high $(TNH + DNH)/C_{30}H$ αβ Hopane ratios, HHI, and gammacerane index (Figs. 2, 3), the intensity of PZE most likely reflected water column sulfate levels. Overall, the above carotenoid patterns through time are attributed to changing sulfate concentrations in the SARBs, where a brackish waterbody with moderate sulfate concentrations prevailed in the Aptian stage.

A transitional Aptian stage is further supported by patterns of sterane/hopane ratios and 2-MHI. The Berr/Bar stage features low sterane/hopane ratios (0.12 ± 0.06), in contrast to ratios mostly >1 in the Aptian and Albian. Low sterane/hopane ratios <1 are commonly observed in lacustrine source rocks and oils[74,75]. Empirically, sterane/hopane ratios are generally high in typical Phanerozoic marine sediments (~0.5 to >2)[27], but may vary largely in brackish environments[64]. High sterane/hopane ratios are attributed to the proliferation of eukaryotic algae under nutrient replete conditions as compared to the preponderance of photo-trophic bacteria in nutrient-depleted lacustrine settings[21,27,28]. Relatively high values and large variability of sterane/hopane ratios in the Aptian stage are thus suggestive of nutrient perturbation from intruded seawater and possibly brackish conditions. Similarly, 2-methylhopanoids have been shown to be prominent when the water column experiences fluctuating redox conditions[33]. The observation of highest 2-MHI values in the Aptian stage is in consensus with seawater incursion-induced redox perturbations, further corroborating our postulation of a transitional brackish waterbody in the Aptian stage.

The "transitional" nature of the Aptian stage and the termination of evaporite deposits by early Albian is consistent with the progressive opening of the SARBs in the Early Cretaceous (Supplementary Note 1). This also reasonably explains the massive Aptian evaporite deposits since a sufficient barrier is required for evaporite deposition in restricted basins[3,4,62], a phenomenon resembling the observation in the modern Red Sea[22]. A large volume of seawater influx into the rift basins is synchronous with a decline in global sea-level in the early Albian[13,62], and converted the SARBs into a semi-restricted marine environment and eased the hypersaline conditions[4,76], as indicated by a decline in gammacerane index values (Fig. 2) and the disappearance of smooth-shelled *Aracajuia* living in stressed environments[8]. As revealed by the empirical proxy of C_{26} tricyclic terpane/(Ts+Tm)[77], water circulation may have initiated upwelling in the SARBs (Fig. 3), which partially broke the water column stratification, enhanced primary production and established the typical Albian carbonate platform systems (Fig. 1).

Implications on biomarker proxies, paleoenvironments and petroleum exploration. Overall, biomarkers have been demonstrated in their effectiveness for distinguishing and reconstructing depositional environments. Brackish and transitional environments influenced considerably by seawater ingression may exhibit chaotic features in faunal compositions, with the juxtaposition of both marine and lacustrine species. In comparison, saline and hypersaline water bodies are typical deprived of the diverse, cosmopolitan faunas that facilitate detailed biostratigraphic assessments and paleoenvironmental reconstructions. In cases like these, molecular fossils are particularly valuable sources of information concerning nonmarine to marine transitions since they document the changes in microbial communities that take place in concert with changes in water chemistry. Whereas our current results for aromatic carotenoid biomarkers make them candidate proxies in discriminating lacustrine from marine depositional settings, the comprehensive biomarker analysis and interpretation as presented in this study may provide insights on facilitating future assessments of paleoenvironmental and palaeoecological shifts of critical geological time periods.

Multiple oceanic anoxic events have been widely reported in open marine environments in the Early Cretaceous[56]. Our results indicate that the phenomena of Early Cretaceous basin anoxia are similarly reflected in transitional and restricted settings. In fact, the reconstruction of redox conditions, as presented in this study, suggests that anoxia and euxinia conditions may have persisted

through the Early Cretaceous Epoch, at least in the SARBs. Additionally, numerous Early Cretaceous anoxia events have been similarly reported in isolated lacustrine basins[78]. Therefore, the co-occurrence of worldwide anoxia in a variety of unconnected basins in Early Cretaceous suggests that there were driven by global processes, possibly tectonics and climates. In consensus with this hypothesis, former studies attributed the cause of Early Cretaceous anoxic events to volcanism-driven release of greenhouse gases, which induced warmer climates and enhanced nutrient supply to the global ocean[79,80]. Additionally, our reconstruction of seawater incursion into SARBs may represent one step further in resolving the orientation and timing of the opening of the South Atlantic Ocean, which could possibly be incorporated into future plate tectonic model simulations.

This study also has general implications on petroleum exploration and exploitation. Given marine signals being conventionally interpreted as post-salt in age[14,66], the discovery of seawater signal in the Aptian strata underlying the Aptian evaporites may help resolve the long-lasting debate on the age diagnostics of the crude oils from this region[67]. By facilitating the projection of oil-source rock correlations, our results thus provide valuable instructions on petroleum exploration along the conjugate margins of the South Atlantic Ocean[7].

Methods

Geological settings and samples. The South Atlantic rift basins (SARBs) are located in between Ascension Fracture Zone and the Rio Grande Rise-Walvis Ridge, and were formed from subsidence in the interior of Gondwana. The tectonic evolution of the SARBs is described in detail in the supplementary file (Supplementary Note 1). A total number of 90 samples were analysed from two cores, the Onango Ezanga-1 core (ONEZ-1) in the Gabon Basin and the Maculungo-1 core (MA-1) in the Kwanza Basin. The stratigraphy was revised from previous publications (Supplementary Note 2), whereas the age models of both drill cores are described in detail in the supplementary file (Supplementary Note 3). Samples are primarily laminated shales, carbonates and sandstones. Forty-one samples from the ONEZ-1 core cover the Berriasian-Barremian to Aptian stages, range in depths from 320.9 to 865.4 m, with 24 and 17 samples from the Berriasian-Barremian and Aptian stages, respectively. The remaining 49 samples were from 1899.47 to 3117 m in the MA-1 core, including 17 and 32 samples from Aptian and Albian stages, respectively. Samples from Berriasian-Barremian stage were primarily cuttings, while the remaining samples were core plugs or chips.

Sample preparation. Sub-samples were sonicated in Milli-Q water and methanol sequentially to clean the exterior and remove any potential contaminants or drilling fluids. After drying in the oven (50 °C), samples were placed in a stainless steel puckmill and powdered using a Shatterbox. Between samples, the puckmill was cleaned by grinding combusted (550 °C) sand, rinsing with Milli-Q water, methanol and dichloromethane, sequentially. Subsequently, samples were measured for total organic matter and carbonate contents (Supplementary Methods).

Total bitumen extraction. Total bitumens were extracted from the powdered rock samples with dichloromethane:methanol (DCM:MeOH; 9:1, v/v), using sonication and centrifugation. After concentration with a gentle nitrogen flow, ~3 ml hexane was added to the extracts to separate the maltene fraction from the asphaltene after sonication and centrifugation. Elemental sulfur was trapped and removed by the addition of activated copper shot. The resulting maltenes were dried to <100 μl and fractionated into non-polar and polar fractions on a silica gel column by using hexane:DCM (4:1, v/v) and DCM:MeOH (4:1, v/v), sequentially.

Instrumental analysis. Non-polar fractions were analysed using an Agilent 7890B gas chromatography (GC) coupled to an Agilent 7010 A triple quadrupole mass spectrometer (GC-MS/MS), equipped with a DB-5MS column (60 m × 250 μm × 0.25 μm). Samples were introduced via a multimode inlet with an initial temperature at 45 °C which was ramped to 340 °C at a rate of 700 °C /min, and held isothermally throughout the run. The GC oven was held at 40 °C for 1.5 min, followed by a ramp of 4 °C/min to 325 °C, then held isothermally for 27 min. The column flow was set to 1.2 ml/min and ramped to 3 ml/min at a rate of 0.02 ml/min. The ramped flow program was adopted to enhance signal-to-noise ratios at high temperature zones. The source and transfer line temperatures were set to 280 °C and 325 °C, respectively. The electron energy was 50 eV. Samples were run under multiple reactions monitoring (MRM) mode using paired precursor-product ions optimized for each compound.

Data analysis. Biomarker results were processed using Masshunter Qualitative and Quantitative software. The calculation of absolute concentrations was not undertaken due to the lack of robust internal standards for each group of compounds. Instead, diagnostic or empirical ratios based on compound peak areas were adopted. Biomarker results were plotted as box-whisker plots for the expression of ranges and distributions, and as crossplots for correlations or covariations. The *t*-test was performed for statistical differences between groups of variables, with $p < 0.05$ indicative of significant differences.

References

1. Wegener, A. Die entstehung der kontinente. *Geologische Rundschau* **3**, 276–292 (1912).
2. Chaboureau, A.-C. et al. Paleogeographic evolution of the central segment of the South Atlantic during Early Cretaceous times: Paleotopographic and geodynamic implications. *Tectonophysics* **604**, 191–223 (2013).
3. Kukla, P. A., Strozyk, F. & Mohriak, W. U. South Atlantic salt basins–witnesses of complex passive margin evolution. *Gondwana Res.* **53**, 41–57 (2018).
4. Pérez-Díaz, L. & Eagles, G. South Atlantic paleobathymetry since early Cretaceous. *Sci. Rep.* **7**, 1–16 (2017).
5. Poropat, S. F. & Colin, J.-P. Early Cretaceous ostracod biostratigraphy of eastern Brazil and western Africa: An overview. *Gondwana Res.* **22**, 772–798 (2012).
6. Behrooz, L. et al. Astronomically driven variations in depositional environments in the South Atlantic during the Early Cretaceous. *Paleoceanogr. Paleoclimatol.* **33**, 894–912 (2018).
7. Brownfield, M. E. & Charpentier, R. R. Geology and total petroleum systems of the west-central coastal province (7203), west Africa). US Geological Survey (2006).
8. Dingle, R. Walvis Ridge Barrier: its influence on palaeoenvironments and source rock generation deduced from ostracod distributions in the early South Atlantic Ocean. *Geological Soc. London Special Publ.* **153**, 293–302 (1999).
9. Harris, N. B., Freeman, K. H., Pancost, R. D., White, T. S. & Mitchell, G. D. The character and origin of lacustrine source rocks in the Lower Cretaceous synrift section, Congo Basin, west Africa. *AAPG Bull.* **88**, 1163–1184 (2004).
10. Thompson, D. L., Stilwell, J. D. & Hall, M. Lacustrine carbonate reservoirs from Early Cretaceous rift lakes of Western Gondwana: Pre-salt coquinas of Brazil and West Africa. *Gondwana Res.* **28**, 26–51 (2015).
11. Szatmari, P. et al. Petrography, geochemistry and origin of South Atlantic evaporites: the Brazilian side. *Marine Petroleum Geology* **127**, 104805 (2021).
12. Lentini, M. R., Fraser, S. I., Sumner, H. S. & Davies, R. J. Geodynamics of the central South Atlantic conjugate margins: implications for hydrocarbon potential. *Petroleum Geosci.* **16**, 217–229 (2010).
13. Bonatti, E. et al. Lower Cretaceous deposits trapped near the equatorial Mid-Atlantic Ridge. *Nature* **380**, 518 (1996).
14. Burwood, R., Leplat, P., Mycke, B. & Paulet, J. Rifted margin source rock deposition: a carbon isotope and biomarker study of a west African Lower Cretaceous "lacustrine" section. *Organic Geochem.* **19**, 41–52 (1992).
15. Arai, M. Aptian/Albian (Early Cretaceous) paleogeography of the South Atlantic: a paleontological perspective. *Braz. J. Geol.* **44**, 339–350 (2014).
16. Bate, R. H. Non-marine ostracod assemblages of the Pre-Salt rift basins of West Africa and their role in sequence stratigraphy. *Geol. Soc. Lond. Spec. Publ.* **153**, 283–292 (1999).
17. Torsvik, T. H., Rousse, S., Labails, C. & Smethurst, M. A. A new scheme for the opening of the South Atlantic Ocean and the dissection of an Aptian salt basin. *Geophys. J. Int.* **177**, 1315–1333 (2009).
18. Karner, G. & Gambôa, L. Timing and origin of the South Atlantic pre-salt sag basins and their capping evaporites. *Geol. Soc. London Spec. Publ.* **285**, 15–35 (2007).
19. Mohriak, W., Nemčok, M. & Enciso, G. South Atlantic divergent margin evolution: rift-border uplift and salt tectonics in the basins of SE Brazil. *Geol. Soc. London Spec. Publ.* **294**, 365–398 (2008).
20. Aksu, A., Hiscott, R. & Yaşar, D. Oscillating Quaternary water levels of the Marmara Sea and vigorous outflow into the Aegean Sea from the Marmara Sea–Black Sea drainage corridor. *Marine Geology* **153**, 275–302 (1999).

21. Ma, J. et al. Biomarkers reveal Eocene marine incursions into the Qaidam Basin, north Tibetan Plateau. *Organic Geochem.* **166**, 104380 (2022).

22. Mohriak, W. U. & Leroy, S. Architecture of rifted continental margins and break-up evolution: insights from the South Atlantic, North Atlantic and Red Sea–Gulf of Aden conjugate margins. *Geological Soc. London Spec. Publ.* **369**, 497–535 (2013).

23. Summons, R. E., Welander, P. V. & Gold, D. A. Lipid biomarkers: molecular tools for illuminating the history of microbial life. *Nat. Rev. Microbiol.* **22**, 174–185 (2021).

24. Fox, C. P. et al. Molecular and isotopic evidence reveals the end-Triassic carbon isotope excursion is not from massive exogenous light carbon. *Proc. Natl. Acad. Sci.* **117**, 30171–30178 (2020).

25. Moldowan, J. M. et al. Sedimentary 24-n-propylcholestanes, molecular fossils diagnostic of marine algae. *Science* **247**, 309–312 (1990).

26. Roussel, A., Cui, X. & Summons, R. E. Biomarker stratigraphy in the Athel Trough of the South Oman Salt Basin at the Ediacaran-Cambrian Boundary. *Geobiology* **18**, 663–681 (2020).

27. Brocks, J. J. et al. The rise of algae in Cryogenian oceans and the emergence of animals. *Nature* **548**, 578–581 (2017).

28. Love, G. D. & Zumberge, J. A. *Emerging patterns in proterozoic lipid biomarker records.* Cambridge University Press (2021).

29. Grabenstatter, J. et al. Identification of 24-n-propylidenecholesterol in a member of the Foraminifera. *Organic Geochem.* **63**, 145–151 (2013).

30. Peters, K. E., Walters, C. C. & Moldowan, J. M. *The Biomarker Guide (2nd Edition).* Cambridge University Press (2005).

31. Rohmer, M., Bouvier-Nave, P. & Ourisson, G. Distribution of hopanoid triterpanes in prokaryotes. *J. Gen. Microbiol.* **130**, 1137–1150 (1984).

32. Summons, R. E., Jahnke, L. L., Hope, J. M. & Logan, G. A. 2-methylhopanoids as biomarkers for cyanobacterial oxygenic photosynthesis. *Nature* **400**, 554–556 (1999).

33. Naafs, B. D. A., Bianchini, G., Monteiro, F. M. & Sánchez-Baracaldo, P. The occurrence of 2-methylhopanoids in modern bacteria and the geological record. *Geobiology* **20**, 41–59 (2022).

34. Elling, F. J. et al. Vitamin B12-dependent biosynthesis ties amplified 2-methylhopanoid production during oceanic anoxic events to nitrification. *Proc. Natl. Acad. Sci.* **117**, 32996–33004 (2020).

35. Summons, R. E., Jahnke, L. L. & Roksandic, Z. Carbon isotopic fractionation in lipids from methanotrophic bacteria: relevance for interpretation of the geochemical record of biomarkers. *Geochim Cosmochim Acta* **58**, 2853–2863 (1994).

36. Welander, P. V. & Summons, R. E. Discovery, taxonomic distribution, and phenotypic characterization of a gene required for 3-methylhopanoid production. *Proc. Natl. Acad. Sci.* **109**, 12905–12910 (2012).

37. French, K. L., Birdwell, J. E. & Berg, V. Biomarker similarities between the saline lacustrine Eocene Green River and the Paleoproterozoic Barney Creek Formations. *Geochimica et Cosmochimica Acta* **274**, 228–245 (2020).

38. Sinninghe Damsté, J. S. et al. Evidence for gammacerane as an indicator of water column stratification. *Geochim Cosmochim Acta* **59**, 1895–1900 (1995).

39. Cui, X. et al. Niche expansion for phototrophic sulfur bacteria at the Proterozoic-Phanerozoic transition. *Proc. Natl. Acad. Sci.* **117**, 17599–17606 (2020).

40. Liaaen-Jensen, S. & Andrewes, A. G. Microbial carotenoids. *Ann. Rev. Microbiol.* **26**, 225–248 (1972).

41. Brocks, J. J. et al. Biomarker evidence for green and purple sulphur bacteria in a stratified Palaeoproterozoic sea. *Nature* **437**, 866–870 (2005).

42. French, K. L., Rocher, D., Zumberge, J. E. & Summons, R. E. Assessing the distribution of sedimentary C40 carotenoids through time. *Geobiology* **13**, 139–151 (2015).

43. Hamilton, T. L. et al. Coupled reductive and oxidative sulfur cycling in the phototrophic plate of a meromictic lake. *Geobiology* **12**, 451–468 (2014).

44. Overmann, J., Cypionka, H. & Pfennig, N. An extremely low-light-adapted phototrophic sulfur bacterium from the black sea. *Limnology Oceanogr.* **37**, 150–155 (1992).

45. Graham, J. E. & Bryant, D. A. The biosynthetic pathway for synechoxanthin, an aromatic carotenoid synthesized by the euryhaline, unicellular cyanobacterium Synechococcus sp. strain PCC 7002. *J. Bacteriol.* **190**, 7966–7974 (2008).

46. Graham, J. E., Lecomte, J. T. J. & Bryant, D. A. Synechoxanthin, an aromatic C40 xanthophyll that is a major carotenoid in the cyanobacterium Synechococcus sp. PCC 7002. *J. Nat. Prod* **71**, 1647–1650 (2008).

47. Hartgers, W. A. et al. A molecular and carbon isotopic study towards the origin and diagenetic fate of diaromatic carotenoids. *Organic Geochem.* **22**, 703–725 (1994).

48. Schaeffer, P., Adam, P., Wehrung, P. & Albrecht, P. Novel aromatic carotenoid derivatives from sulfur photosynthetic bacteria in sediments. *Tetrahedron Lett.* **38**, 8413–8416 (1997).

49. Maresca, J., Graham, J. & Bryant, D. The biochemical basis for structural diversity in the carotenoids of chlorophototrophic bacteria. *Photosynthesis Res.* **97**, 121–140 (2008).

50. Behrens, A., Schaeffer, P., Bernasconi, S. & Albrecht, P. Mono- and bicyclic squalene derivatives as potential proxies for anaerobic photosynthesis in lacustrine sulfur-rich sediments. *Geochimica et Cosmochimica Acta* **64**, 3327–3336 (2000).

51. Sandmann, G. Carotenoid biosynthesis and biotechnological application. *Arch. Biochem. Biophys.* **385**, 4–12 (2001).

52. Pedentchouk, N., Freeman, K. H., Harris, N. B., Clifford, D. J. & Grice, K. Sources of alkylbenzenes in Lower Cretaceous lacustrine source rocks, West African rift basins. *Organic Geochem.* **35**, 33–45 (2004).

53. Bate, R. H., Cameron, N. R. & Brandao, M. G. The lower cretaceous (pre-salt) lithostratigraphy of the Kwanza basin, Angola. *Newsletters on Stratigraphy*, 117-127 (2001).

54. Davison, I. Geology and tectonics of the South Atlantic Brazilian salt basins. *Geol. Soc. London Special Publ.* **272**, 345–359 (2007).

55. Tedeschi, L. R. et al Aptian carbon-isotope record from the Sergipe-Alagoas Basin: New insights into oceanic anoxic event 1a and the timing of seawater entry into the South Atlantic. *Newsletters on Stratigraphy*, (2019).

56. Tedeschi, L. R. et al. New age constraints on Aptian evaporites and carbonates from the South Atlantic: Implications for Oceanic Anoxic Event 1a. *Geology* **45**, 543–546 (2017).

57. Matos, R., Krueger, A., Norton, I. & Casey, K. The fundamental role of the Borborema and Benin–Nigeria provinces of NE Brazil and NW Africa during the development of the South Atlantic Cretaceous Rift system. *Marine Petroleum Geology* **127**, 104872 (2021).

58. Szatmari, P. & Milani, E. J. Tectonic control of the oil-rich large igneous-carbonate-salt province of the South Atlantic rift. *Marine Petroleum Geology* **77**, 567–596 (2016).

59. Meyer, K. M. et al. Carotenoid biomarkers as an imperfect reflection of the anoxygenic phototrophic community in meromictic Fayetteville Green Lake. *Geobiology* **9**, 321–329 (2011).

60. Gasperini, L. et al. Lower Cretaceous to Eocene sedimentary transverse ridge at the Romanche Fracture Zone and the opening of the equatorial Atlantic. *Marine Geology* **176**, 101–119 (2001).

61. Gallo, V. & Coelho, P. M. First occurrence of an aulopiform fish in the Barremian of the Sergipe-Alagoas Basin, northeastern Brazil. *Mesozoic fishes* **4**, 351–371 (2008).

62. Burke, K. & Sengör, A. C. Ten metre global sea-level change associated with South Atlantic Aptian salt deposition. *Marine Geology* **83**, 309–312 (1988).

63. Nunn, J. A. & Harris, N. B. Subsurface seepage of seawater across a barrier: A source of water and salt to peripheral salt basins. *Geol. Soc. Am. Bull.* **119**, 1201–1217 (2007).

64. Xu, H., George, S. C. & Hou, D. The occurrence of isorenieratane and 24-n-propylcholestanes in Paleogene lacustrine source rocks from the Dongying Depression, Bohai Bay Basin: Implications for bacterial sulfate reduction, photic zone euxinia and seawater incursions. *Organic Geochem.* **127**, 59–80 (2019).

65. Bastos, L. P. H. et al. Organic geochemical evidence for the transition of Aptian-Albian hypersaline environments into marine restricted seas: The South Atlantic oceanic northern gateway and its implications for the pre-salt deposits. *Marine Petroleum Geology* **140**, 105632 (2022).

66. Burwood, R. Angola: source rock control for Lower Congo Coastal and Kwanza Basin petroleum systems. *Geological Society London Special Publ.* **153**, 181–194 (1999).

67. Schiefelbein, C., Zumberge, J., Cameron, N. & Brown, S. AAPG Memoir 73, Chapter 2: Geochemical Comparison of Crude Oil Along the South Atlantic Margins. (2000).

68. Lovley, D. R., Dwyer, D. F. & Klug, M. J. Kinetic analysis of competition between sulfate reducers and methanogens for hydrogen in sediments. *Appl. Environ. Microbiol.* **43**, 1373–1379 (1982).

69. Davison, I., Anderson, L. & Nuttall, P. Salt deposition, loading and gravity drainage in the Campos and Santos salt basins. *Geological Soc. London Spec. Publ.* **363**, 159–174 (2012).

70. Schoell, M., McCaffrey, M., Fago, F. & Moldowan, J. Carbon isotopic compositions of 28, 30-bisnorhopanes and other biological markers in a Monterey crude oil. *Geochimica et Cosmochimica Acta* **56**, 1391–1399 (1992).

71. Wagner, T. & Pletsch, T. No major thermal event on the mid-Cretaceous Côte d'Ivoire–Ghana Transform Margin. *Terra Nova* **13**, 165–171 (2001).

72. Friedrich, O., Erbacher, J. & Mutterlose, J. Paleoenvironmental changes across the Cenomanian/Turonian boundary event (oceanic anoxic event 2) as indicated by benthic foraminifera from the Demerara Rise (ODP Leg 207). *Revue de micropaléontologie* **49**, 121–139 (2006).

73. Müller, R. D. et al. A global plate model including lithospheric deformation along major rifts and orogens since the Triassic. *Tectonics* **38**, 1884–1907 (2019).

74. Ding, W., Hou, D., Jiang, L., Jiang, Y. & Wu, P. High abundance of carotanes in the brackish-saline lacustrine sediments: A possible cyanobacteria source? *Int. J. Coal Geology* **219**, 103373 (2020).

75. Summons, R. E., Hope, J. M., Swart, R. & Walter, M. R. Origin of Nama Basin bitumen seeps: Petroleum derived from a Permian lacustrine source rock traversing southwestern Gondwana. *Organic Geochem.* **39**, 589–607 (2008).

76. Naafs, B. & Pancost, R. D. Environmental conditions in the South Atlantic (Angola basin) during the Early Cretaceous. *Organic Geochem.* **76**, 184–193 (2014).

77. Zumberge, J., Illich, H. & Waite L. Petroleum geochemistry of the Cenomanian–Turonian Eagle Ford oils of south Texas. (2016).

78. Zhang, X., Li, S., Wang, X., Zhao, X. & Yin, T. Expression of the early Aptian Oceanic Anoxic Event (OAE) 1a in lacustrine depositional systems of East China. *Global Planet. Change* **196**, 103370 (2021).

79. Matsumoto, H. et al. Marine Os isotopic evidence for multiple volcanic episodes during Cretaceous Oceanic Anoxic Event 1b. *Sci. Rep.* **10**, 1–10 (2020).

80. Méhay, S. et al. A volcanic CO_2 pulse triggered the Cretaceous Oceanic Anoxic Event 1a and a biocalcification crisis. *Geology* **37**, 819–822 (2009).

Acknowledgements

Author contributions

X.C. and R.E.S. designed the research; K.H.F. provided the core samples; X.C. performed the geochemical analyses; X.C. and R.E.S. analyzed the data; and X.C., B.W., K.H.F., and R.E.S. wrote the manuscript.

Competing interests

The authors declare no competing interests.

Additional information

Supplementary information The online version contains supplementary material available at https://doi.org/10.1038/s43247-022-00668-3.

Correspondence and requests for materials should be addressed to Xingqian Cui or Roger E. Summons.

Peer review information *Communications Earth & Environment* thanks David Naafs, Simon Brassell and the other, anonymous, reviewer(s) for their contribution to the peer review of this work. Primary Handling Editors: Sze Ling Ho, Joe Aslin, Heike Langenberg. Peer reviewer reports are available.

Reprints and permission information is available at http://www.nature.com/reprints

Publisher's note Springer Nature remains neutral with regard to jurisdictional claims in published maps and institutional affiliations.